Article

Assessment of the Feasibility of Applying the Electromagnetic Time Reversal Theory to Locate Defects in Grounding Electrodes

Rafael Alipio [1,2,*], Naiara Duarte [1], Hamidreza Karami [3], Marcos Rubinstein [3] and Farhad Rachidi [1,*]

1   Electromagnetic Compatibility Laboratory, Swiss Federal Institute of Technology Lausanne (EPFL),
    1015 Lausanne, Switzerland; naiara.duarte@epfl.ch
2   Department of Electrical Engineering, CEFET-MG—Federal Center of Technological Education of Minas
    Gerais, Av. Amazonas, 7675, Nova Gameleira, Belo Horizonte 30510-000, Minas Gerais, Brazil
3   Institute for Information and Communication Technologies, University of Applied Sciences Western
    Switzerland, 1400 Yverdon-les-Bains, Switzerland; hamidreza.karami@heig-vd.ch (H.K.);
    marcos.rubinstein@heig-vd.ch (M.R.)
*   Correspondence: rafael.alipio@epfl.ch (R.A.); farhad.rachidi@epfl.ch (F.R.)

Abstract: In recent years, the electromagnetic time reversal (EMTR) theory has been successfully applied for locating various sources of disturbances, such as short-circuit faults, in power systems. In this paper, a theoretical analysis of the feasibility of applying EMTR to locate defects (corrosion and break points) in grounding systems is presented. An EMTR algorithm to locate faults in buried grounding wires is proposed and a comprehensive analysis with respect to some salient influencing parameters, for instance, the ground conductivity, medium losses, the defect location and type (soft or hard), is carried out. According to the obtained results, the proposed method appears to be very promising for real applications. The need for experimental validation to confirm the applicability of this method is emphasized.

Keywords: electromagnetic time reversal; grounding systems; defect location; break points; electrode corrosion; telegrapher's equations

1. Introduction

Grounding systems play a fundamental role in power systems and are responsible for providing a low-impedance path to earth for fault currents and, at the same time, ensuring a smooth distribution of potentials at the ground level to reduce the risk of a person in the vicinity of grounded facilities being exposed to the danger of critical electric shock [1]. According to most standards, copper is the main material considered for grounding electrodes [1–3]. More recently, galvanized steel has also been used to construct substation grounding grids and transmission line tower-foot grounding systems, taking advantage of its low cost [4–6]. Such a design, however, requires special attention to the corrosion of the steel. The corrosion process is primarily determined by the physical and chemical properties of the soil in which the electrodes are buried, although other factors, such as unqualified joints during construction, also play a role [7]. In general, the corrosion of steel grounding electrodes is a serious issue, and can result in damage to the electrodes and, in critical cases, can lead to breakpoints, deteriorating the performance of the grounding system.

In this context, but not exclusively, the fault diagnosis of grounding systems is very important and can help anticipate the punctual maintenance of degraded electrodes and prevent the electrical system from becoming susceptible to risks due to the deterioration of the grounding system. A common practice is the measurement of some indirect parameters that can assess the status of the grounding system, for example, the grounding resistance [4]. Although this method can indicate—albeit with limited accuracy—that there is something wrong with the grounding system, the information obtained is not enough to locate the

defect points. In this case, the only way to locate such points would be to dig up the entire grounding system and perform a point-by-point inspection, which is obviously a blind search that is laborious, expensive and that can itself cause further damage to the grounding system.

Other existing approaches for diagnosing defects in grounding systems are summarized as follows.

The "electromagnetic method" is based on measuring the magnetic field produced at the ground surface using the conductors of the grounding system under test in response to either the injection of a current or the application of an excitation magnetic field above the region where the electrodes are buried [6,8–11]. The method relies on the hypothesis that grounding electrodes in different states produces different magnetic fields on the earth's surface and such a modification in the produced field could be used to identify fault points in the grounding system. In the case of current injection, the current magnitude must usually be high, in the order of hundreds of amperes, which may require specific equipment, in addition to demanding strict personal safety constraints. In the case of applying a magnetic field in the region where the grounding system is installed, it might be difficult and laborious to guarantee that the moving route during the measurements is consistent with the location of the buried electrodes. Furthermore, in both cases, the method's accuracy is limited by the used magnetic field sensors, which may be strongly affected by the electromagnetic fields generated by the electrical system itself, depending on the type and/or voltage level of the facility under test.

Electrochemical methods are based on the determination of the corrosion rate of the electrodes through measurements or corrosion simulation models [7,12]. Given the highly heterogeneous characteristics of soil, the determination of this rate may contain a high degree of uncertainty, especially in the case of large grounding systems that are covered under soils with different characteristics. In addition, although the method can be used to roughly predict the corrosion state of a grounding system, it is not applicable for effectively locating potential defect points.

The so-called network method is based on the idea that the grounding system can be seen as a circuit network, where each conductor is a branch and each crossing point between conductors is a node [13,14]. The resistance between two nodes of the grounding system can be measured, provided that they can be accessed, for example, via down-lead conductors. Then, monitoring the value of this resistance, called port resistance, can be used to assess the state of the grounding system via a network model. An important limitation of the method is the need for several down-lead conductors to access the grounding nodes in order to obtain accurate diagnostics. Additionally, depending on the degree of the defect in the grounding system, the modifications introduced in the measured port resistance can be quite small, making it difficult to determine an assertive diagnosis.

In light of the foregoing considerations, this paper aims at investigating the feasibility of applying the theory of time reversal (TR) to the problem of fault location in buried grounding wires. The TR method was first developed in the field of acoustics [15–17] and it was later extended to electromagnetism using the acronym EMTR (electromagnetic time reversal) [18]. The EMTR method take advantage of the time reversibility of the wave equation. More specifically, when the observed electromagnetic disturbances in specific observation points of the system are time reversed and back-injected into the original system, they refocus back on the source of the disturbance. The considered applications of EMTR include locating lightning flashes (e.g., [19]), short-circuit faults (e.g., [20–23]), lightning strikes and flashovers [24], series faults and partial discharges in coaxial line networks and transformers (e.g., [25–29]). However, to the best of the authors' knowledge, this is the first time that EMTR is applied to locate faults in bare wires immersed in a lossy medium (ground).

The structure of this paper is as follows. Section 2 presents the modeling of grounding electrodes with series faults (defects) together with a first assessment of the impact of such a fault on the input grounding impedance. In Section 3, we present the principles of the

proposed time reversal procedure for fault detection and localization in grounding electrodes. In Section 4, test cases are described, and in Section 5, the results of a comprehensive sensitivity analysis on the feasibility of applying the EMTR method to locate defects in grounding electrodes are presented. A discussion and summary of the main conclusions and findings of this study are presented in Section 6.

2. Modeling Grounding Electrodes with Series Faults

2.1. Modeling Based on the Transmission Line (TL) Theory

Figure 1 illustrates a horizontal grounding electrode of length ℓ with a series fault at a distance of ℓ_1 from its left end. The fault is represented by a damaged section of the electrode of length ℓ_f, and the degree of damage can be classified as soft, for example, an initial corrosion process, or hard, associated with an advanced corrosion process or even a breakpoint. For modeling the problem, the transmission line (TL) theory is used, and the faulty electrode is represented through a cascade of three transmission lines of lengths ℓ_1, ℓ_f and $\ell_2 = \ell - \ell_1 - \ell_f$, as indicated in Figure 1. The spatial distribution of voltage $V(x, \omega)$ and current $I(x, \omega)$ along each line section for a given frequency ω is described using the telegrapher's equations:

$$\frac{dV(x, \omega)}{dx} = -(z_{int} + j\omega l) \cdot I(x, \omega), \tag{1}$$

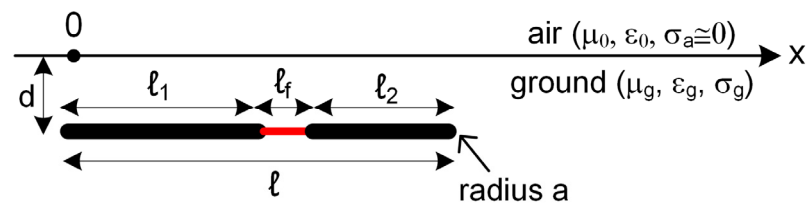$$\frac{dI(x, \omega)}{dx} = -(g + j\omega c) \cdot V(x, \omega). \tag{2}$$

Figure 1. Horizontal grounding electrode with a series fault.

In (1), z_{int} and l are, respectively, the per-unit-length (pul) internal impedance (due to the magnetic field within the electrode) and inductance (due to the magnetic field in the soil) of the grounding electrode. In (2), g and c are, respectively, the pul shunt conductance and capacitance due to the electric field in the soil. The conductance g is computed using the expression proposed by Sunde for a buried horizontal wire given by [30]

$$g = \pi\sigma_g \left[\log\left(\frac{2\ell}{\sqrt{2ad}}\right) - 1 \right]^{-1}, \tag{3}$$

where σ_g is the ground conductivity, ℓ is the electrode length, a is the electrode radius and d is the depth of the electrode. Assuming a homogeneous medium, the pul capacitance of the electrode is simply calculated as

$$c = (\varepsilon_g / \sigma_g) g, \tag{4}$$

where ε_g is the ground permittivity.

The pul inductance of the grounding electrode is calculated using the following expression proposed by King [31]

$$l = \frac{\mu_g}{2\pi} \left[\log\left(\frac{2\ell}{\sqrt{2ad}}\right) - 1 \right], \tag{5}$$

where μ_g is the ground permeability. Finally, the internal impedance is computed considering the exact solution for the internal impedance of a solid cylindrical conductor [32].

It is worth mentioning that the use of the TL theory for modeling horizontal grounding electrodes, assuming the calculation of the parameters applying (3)–(5), was shown in [33] to provide sufficiently accurate results, taking as reference a full-wave method of moments approach. Finally, the spatial distribution of the voltage and current along the faulty electrode shown in Figure 1 can be determined by solving the telegraphers' Equations (1) and (2) for each electrode section and incorporating the appropriate terminal conditions.

2.2. Computational Modeling

Taking as a reference Figure 1, the faulty electrode is modelled as a nonuniform transmission line, which is represented through a cascade of three line sections. Each section is characterized by a two-port model considering a Y-parameter representation. The Y (admittance) parameters relate the terminal currents to the terminal voltages and are defined as [34]

$$\begin{bmatrix} I(0) \\ -I(\ell_S) \end{bmatrix} = \begin{bmatrix} Y_s & Y_m \\ Y_m & Y_s \end{bmatrix} \begin{bmatrix} V(0) \\ V(\ell_S) \end{bmatrix}, \tag{6}$$

where ℓ_S is the line section length and the parameters Y_s and Y_m are given by

$$Y_s = \frac{1}{Z_c} \frac{1}{tanh(\gamma \ell_S)}, \tag{7}$$

$$Y_m = -\frac{1}{Z_c} \frac{1}{\sinh(\gamma \ell_S)}. \tag{8}$$

In (7) and (8), Z_c and γ are, respectively, the characteristic impedance and the propagation constant associated with the k-th section denoted as

$$Z_c = \sqrt{\frac{z_{intk} + j\omega l_k}{g_k + j\omega c_k}}, \tag{9}$$

$$\gamma = \sqrt{(z_{intk} + j\omega l_k)(g_k + j\omega c_k)}, \tag{10}$$

where z_{intk}, l_k, g_k and c_k are, respectively, the pul internal impedance, inductance, conductance and capacitance of the k-th line section.

Considering the series connection between the line sections, a global admittance matrix representation can be obtained as

$$I_E = Y_G \cdot V_n, \tag{11}$$

where I_E is the vector of the injected currents, V_n is the vector of the nodal voltages and Y_G is the global admittance matrix given as a combination of the admittance matrices of each line section as detailed in [34,35]. Assuming the configuration shown in Figure 1, I_E and V_N are 4×1 and Y_G is 4×4. Figure 2 schematically illustrates the representation adopted for the faulty electrode. It is noteworthy that a similar approach could be adopted assuming more than one faulty electrode section.

The presented equations were implemented in a computational code in MATLAB and its consistency was tested considering several benchmark examples of the frequency response of nonuniform transmission lines [34,35].
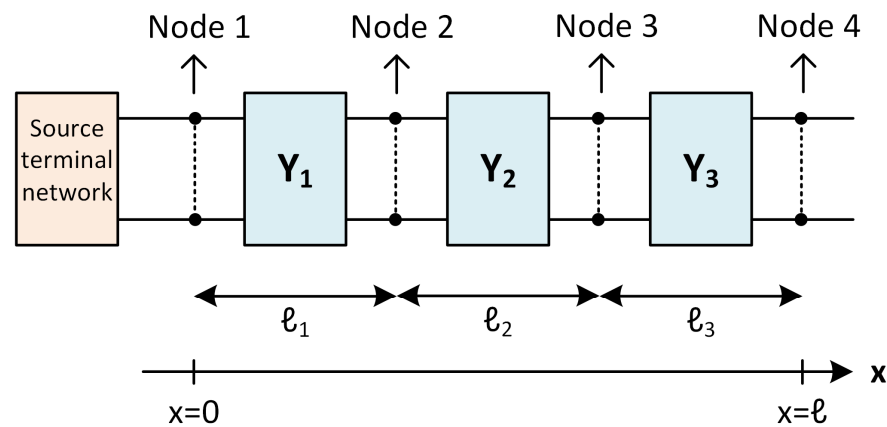
Figure 2. Modeling of the faulty electrode as a nonuniform transmission line represented as a cascade of uniform line sections.

2.3. A First Assessment of the Impact of a Series Fault in Grounding Electrodes

In order to carry out a first assessment of the impact of a series fault on the performance of a grounding electrode, the input impedance of a faulty electrode can be compared with that of a healthy one. The input grounding impedance is defined as the ratio of the phasors of the voltage at the feed point and the injected current in a given frequency range of interest [36]. If a harmonic current of 1 A is injected at the left end of the electrode shown in Figure 1 and the resulting voltage at the feed point $V(\omega)$ is determined, then the grounding input impedance is computed as

$$Z_{in}(\omega) = \frac{V(\omega)}{1\,\text{A}}. \tag{12}$$

To evaluate the impact of a series fault on $Z_{in}(\omega)$, a 50-m long, 7 mm radius electrode composed of steel ($\rho_c = 2.5 \times 10^{-7}$ Ω·m) buried at 1 m depth in soil characterized by $\sigma_g = 4$ mS/m, $\varepsilon_g = 10\varepsilon_0$ and $\mu_g = \mu_0$ is assumed, where ε_0 and μ_0 are, respectively, the vacuum permittivity and permeability.

Generally, two main categories of defects (faults) in grounding electrodes are considered: hard faults (breakpoints), which produce an important impedance discontinuity, and soft faults (corrosion processes that might introduce modifications in the electrode section and material), which lead to a less significant impedance discontinuity and are more difficult to detect. In this paper, the hard faults were modeled simply as an open circuit, while the soft faults were modeled by means of a small modification to the cross-sectional area of the faulty electrode section.

Two types of faults, both at the midpoint of the electrode ($x = 25$ m), are considered: (i) a soft fault, modeled by a 10 cm long damaged section with the equivalent radius reduced from 7 mm to 5 mm (a reduction of approximately 50% in the equivalent cross-sectional area of the electrode) and (ii) a hard fault, corresponding to a breakpoint. The soft fault could be associated with a decrease in the cross-sectional area of the electrode and an increase in its resistivity due to an initial or intermediate corrosion process.

Figure 3 shows the simulated grounding input impedance in the frequency range between 10 Hz and 10 MHz, considering a nonfaulty electrode, labeled "NF electrode", and electrodes with soft and hard faults, labeled "SF electrode" and "HF electrode", respectively. The frequency range was defined in order to cover the different types of transient phenomena to which a grounding system could be subjected, and which have different representative frequencies; for example, short-circuits (low frequencies) and lightning transients (high frequencies).
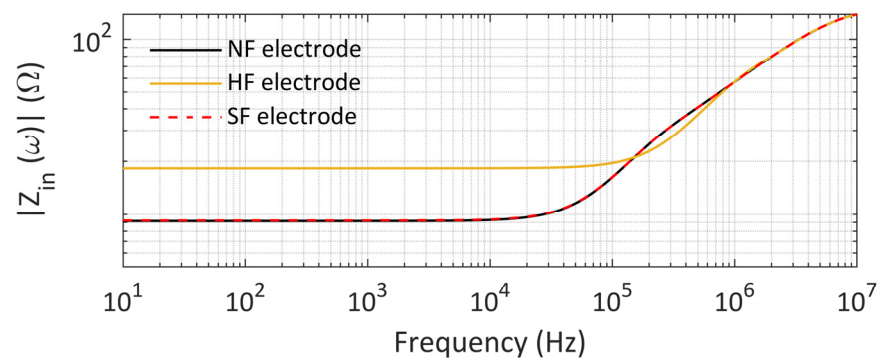
Figure 3. Comparison between the magnitude of the input impedance computed for a grounding electrode without defect (NF) and for electrodes with soft (SF) and hard (HF) series faults.

According to the results, in the case of the hard fault, a significant difference is observed between the calculated input impedance for the nonfaulty and faulty electrodes, with an increase in the magnitude of the latter's impedance in the low-frequency range. As the frequency increases, the difference between the two curves tends to decrease, and in the high-frequency region of the spectrum, they basically overlap. This stems from the fact that, with increasing the frequency, the effect of losses becomes more significant, and only a limited length of the electrode (the so-called effective length) closer to the feed point is seen by the injected current, presumably shorter than 25 m.

By analyzing the results obtained for the soft fault, it is seen that the modification it introduced in the input impedance, compared to the nonfaulty electrode, is negligible. In reality, the two curves are basically indistinguishable, and any difference between them would possibly be of the same order of magnitude as the input impedance measurement uncertainty in a practical application. This result highlighted the fact that, unless additional terminals for current injection very close to the fault point are available, it would be quite difficult not only to locate the fault point, but also to assertively identify the existence or absence of a defect in the grounding electrode using conventional techniques.

3. Electromagnetic Time Reversal Applied to Locate Faults in Grounding Electrodes

A detailed discussion of the time-reversal invariance property of physical systems, along with its application to a variety of problems in EMC and power systems, can be found in [18]. A system is time reversal invariant with respect to a physical quantity if, given a solution $f(t)$ of its governing differential equations, the time-reversed function $g(t)$ given by (13) is also a solution.

$$g(t) = f(-t + k),\tag{13}$$

where k is a constant related to the arbitrary reference origin for the time.

It can be shown that the differential equations describing the voltage/current wave propagation along a lossless transmission line are invariant under a time reversal transformation [20]. Thus, for example, let $f(t)$ be the resultant voltage at one end of a transmission line produced by some source at a given point along it. Given the time reversal invariance property, if the time-reversed signal $g(t)$ is back-injected at the same end of the TL where $f(t)$ was determined, the signal will retrace the path followed in the immediate past and converge to the source of $f(t)$.

Considering the grounding electrode shown in Figure 1, if a signal is applied to its left end, any impedance discontinuity created by a series fault can be seen as a secondary source producing a transmitted wave and a reflected wave. Thus, a TR process can be applied to locate the defect. In Section 3.1 below, a basic time reversal procedure for fault detection and localization in grounding electrodes is described. In Section 3.2, the issue of losses, which are not negligible in the case of bare conductors buried in the ground, is addressed.

3.1. EMTR-Based Algorithm to Locate Faults in Grounding Electrodes

In the proposed EMTR algorithm, to locate defects in a grounding electrode, it is assumed that its basic characteristics, namely, electrode radius and length, are known from the design information. Additionally, the electromagnetic properties of the soil are assumed to be known. Figure 4 illustrates the proposed procedure based on EMTR, which consists of three main steps.
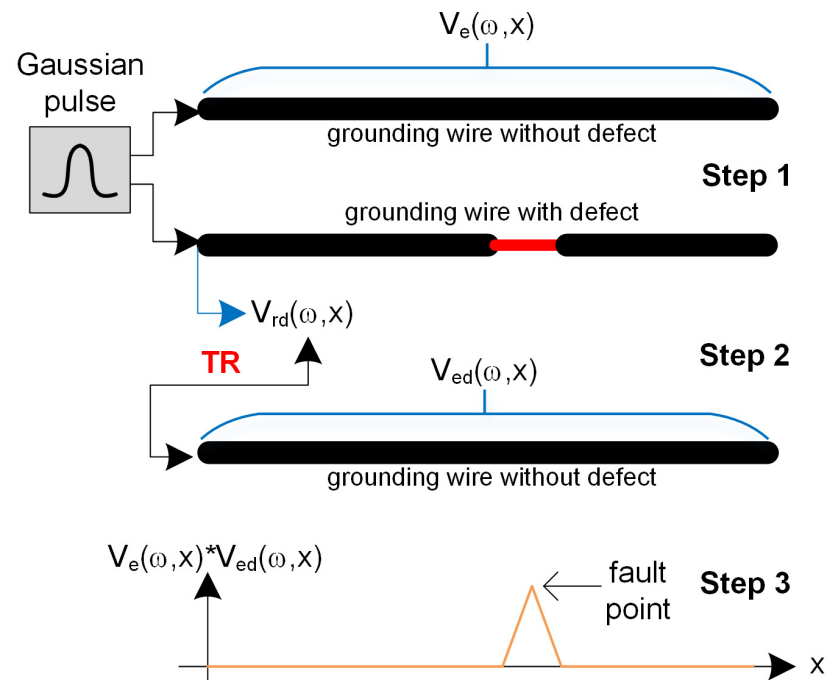

Figure 4. Basic steps of the EMTR-based algorithm to locate faults in grounding electrodes.

In the first step, a voltage Gaussian pulse is applied to the left end of the electrode without a defect, and the spatial voltage distribution $V_e(\omega, x)$ along the electrode is computed using the model based on the TL theory described in Section 2. The same Gaussian pulse is applied to the electrode with a defect and the reflected signal $V_{rd}(\omega)$ is determined. The latter signal is generally obtained through a measurement on the potentially faulty grounding electrode under test. It is worth noting that the reflection coming from the open end of the electrode can be filtered out knowing the electrode length.

In the second step, the reflected signal $V_{rd}(\omega)$ is time-reversed and back-injected through numerical simulation into the grounding electrode without a defect. In the frequency domain, the TR operator is represented by the complex conjugate of the Fourier transform of the signal. Then, the spatial voltage distribution $V_{ed}(\omega, x)$ along the electrode in response to $V_{rd}^*(\omega)$, where $*$ denotes the complex conjugate operator, is numerically computed.

In the last step, a product, corresponding to convolution in the time domain, between the functions $V_e(\omega, x)$ and $V_{ed}(\omega, x)$ is performed for each point x along the electrode. The result of the convolution can be interpreted as a measure of the area overlapping between the two functions. Considering the time reversal operation carried out in the second step, the convolution is expected to reach a maximum at the point along the electrode that presents an associated time delay equal to the time delay of the reflected wave from the fault point.

3.2. The Issue of Losses and Back-Propagation Models

The propagation constant along the grounding electrode can be computed considering the parameters given in (3)–(5) as

$$\gamma_e = \sqrt{(z_{int} + j\omega l)\cdot(g + j\omega c)} = \alpha + j\frac{\omega}{v_f},$$ (14)

where α is the attenuation constant and v_f is the phase velocity. Due to the losses, which are generally frequency-dependent, the propagating signals along the grounding wire experience both attenuation and distortion.

As detailed in [21], the telegrapher's equations are not rigorously time reversal invariant if the line is immersed in a dissipative medium. In the case of a bare wire buried in the ground, the losses are closely related to the soil conductivity, being more significant the higher the conductivity. In an attempt to deal with the issue of losses in the proposed EMTR procedure to locate series faults in grounding electrodes, three back-propagation (BP) models are considered [21]: inverted-loss, lossless and lossy.

The inverted-loss back-propagation model is implemented by changing the sign of the real part of the propagation constant, i.e.,:

$$\widetilde{\gamma}_e = -\alpha + j\frac{\omega}{v_f},$$ (15)

where $\widetilde{\gamma}_e$ is the adopted propagation constant for the back-propagation step. Note that this is not a physical model, since the electrode itself became active and provided energy to the signal that is propagating along it. However, this model can be numerically implemented. In this case, it can be shown that the telegrapher's equations are time reversal invariant.

In the lossless model, the losses in the back-propagation step are disregarded and the resulting propagation constant is given by

$$\widetilde{\gamma}_e = j\frac{\omega}{v_f},$$ (16)

where the phase velocity is assumed to be frequency-independent and equal to $v_f = \frac{c}{\sqrt{\varepsilon_{rg}}}$, where c is the speed of light and ε_{rg} is the relative permittivity of the soil.

Lastly, in the lossy model, the ground losses are included in the back-propagation step and the propagation constant $\widetilde{\gamma}_e$ is assumed to be equal to γ_e, given by (14). Even though a lossy medium is not time-reversal invariant, in [21] this model was shown to lead to accurate results in locating faults on overhead lines.

4. Tested Cases

In order to assess the feasibility of applying the EMTR technique described in Section 3 to locate faults in grounding wires under practical conditions, a comprehensive sensitivity analysis with respect to some salient influencing parameters is performed through numerical simulations. In the analysis, as in the example used in Section 2.2, a 50-m long, 7 mm radius horizontal grounding electrode buried at 1 m depth is considered. Two soil conductivities are assumed, $\sigma_g = 4$ mS/m and $\sigma_g = 0.4$ mS/m; in all simulations, $\varepsilon_g = 10\varepsilon_0$ and $\mu_g = \mu_0$. Taking as a reference Figure 1, two fault points are tested: one near the left end of the electrode at $x = 10$ m and another at the midpoint of the electrode at $x = 25$ m. Finally, for each fault point, two types of faults are considered, namely, a soft and a hard fault, modeled in the same way as described in Section 2.2.

For the sake of simplicity in assessing the feasibility of the method, a homogeneous soil was considered. The assumed values of soil conductivity can be interpreted as the apparent conductivity seen by the grounding electrode buried in a stratified soil; that is, the equivalent homogeneous soil in which the grounding electrode presents a similar behavior as if it was buried in the original stratified soil. A consideration of the stratified soil can be

incorporated into the proposed approach, since the EMTR method can straightforwardly deal with inhomogeneous media, as shown in [20,22].

In this study, we consider three different Gaussian pulses with maximum representative frequencies of approximately 1, 5 and 10 MHz. The Fourier transform of a Gaussian pulse is given by

$$G(\omega) = \tau\sqrt{\pi}\exp\left(-\frac{\tau^2\omega^2}{4}\right), \tag{17}$$

where the parameter τ is adjusted according to the maximum desired representative frequency f_{max} as

$$\tau = \frac{\sqrt{2.3}}{\pi f_{max}}. \tag{18}$$

For each tested case, the product between $V_e(\omega, x)$ and $V_{ed}(\omega, x)$ is normalized and plotted as a function of the position x along the electrode. This normalized product will simply be called "normalized energy".

Table 1 presents a summary of the tested cases.

Table 1. Summary of the tested cases.

Parameter	Details
Electrode geometry	50 m long, 7 mm radius horizontal grounding electrode buried at 1 m depth
Soil parameters	$\sigma_g = 4$ mS/m and $\sigma_g = 0.4$ mS/m, $\varepsilon_g = 10\varepsilon_0$ and $\mu_g = \mu_0$
Fault points	$x = 10$ m and $x = 25$ m
Applied signals	Gaussian pulses of frequencies of 1, 5 and 10 MHz

5. Results

In this section, we report the sensitivity analysis performed to assess the feasibility of the EMTR-based algorithm proposed to locate faults in grounding electrodes. Firstly, in Section 5.1, the accuracy of each assumed BP model is evaluated. In Section 5.2, the influence of the frequency content of the injected pulse on the accuracy and resolution in the fault location provided by the algorithm is discussed. In Section 5.3, the proposed algorithm is tested considering different fault point locations. Finally, in Section 5.4, the issue of locating soft faults is addressed.

5.1. Assessment of the Issue of Losses

Figure 5 shows the obtained results for a hard fault at the midpoint of the electrode, assuming the injection of a 10 MHz Gaussian pulse, and considering the three back-propagation models, namely, the inverted-loss model (labeled as "inverted-loss BP"), the lossless model (labeled as "lossless BP") and the lossy model (labeled as "lossy BP"). The results are presented for soil conductivities of 4 mS/m and 0.4 mS/m.

According to Figure 5a, for the 4-mS/m soil, where the losses are more pronounced, the inverted-loss back-propagation model was able to locate the fault at the correct position (25 m). On the other hand, the lossless and lossy back-propagation models were not able to accurately locate the fault. As seen in Figure 5b, for the 0.4-mS/m soil, the inverted-loss and lossy BP models led to similar results and were able to locate the fault point correctly, while the lossless model, again, was not able to identify the location of the defect.

As expected, the losses have an important influence on the EMTR fault location accuracy. From the results, it was seen that the inverted-loss model for the back-propagation resulted in an accurate estimate of the fault location and, therefore, from this point on, it is assumed for the back-propagation step in the other evaluations of this paper.
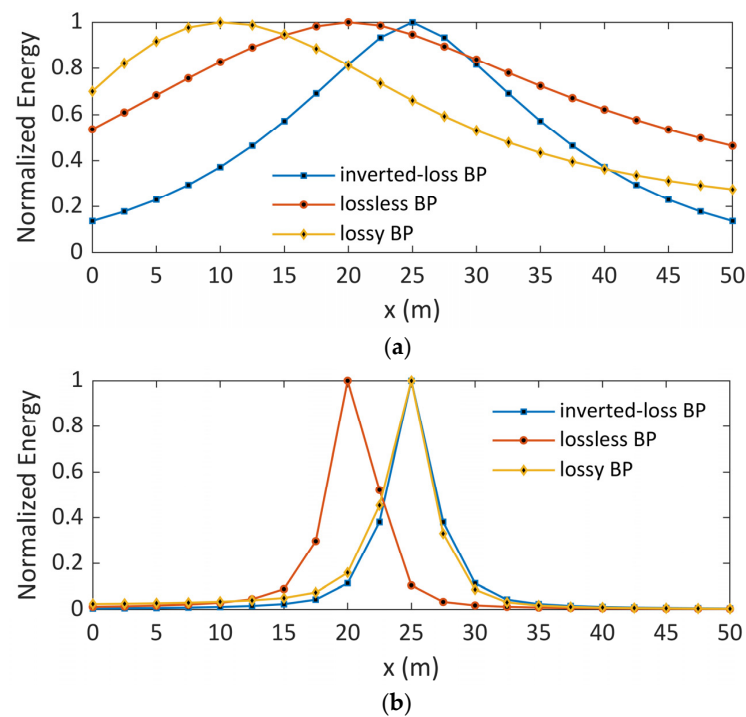
Figure 5. Normalized energy as a function of the position along the electrode for the three back-propagation models and soil conductivities of (**a**) 4 mS/m and (**b**) 0.4 mS/m.

5.2. Influence of the Frequency of the Injected Pulse

Figure 6 shows the obtained results for a hard fault at the midpoint of the electrode, assuming the injection of Gaussian pulses of different frequencies, namely, 1, 5 and 10 MHz, and assuming soil conductivities of 4 mS/m and 0.4 mS/m.
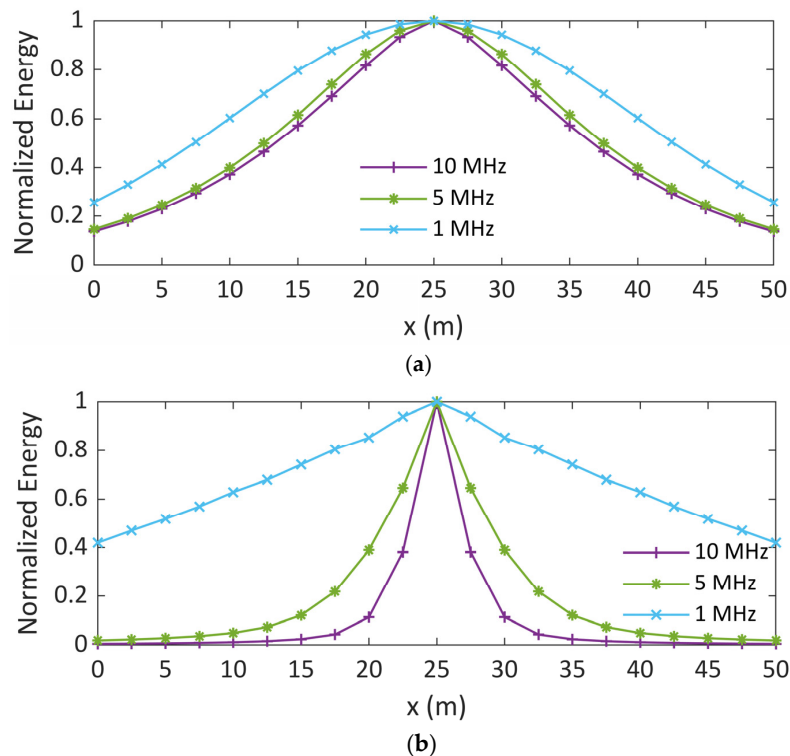

Figure 6. Normalized energy as a function of the position along the electrode considering the injection of Gaussian pulses of different frequencies and soil conductivities of (**a**) 4 mS/m and (**b**) 0.4 mS/m.

According to the results, increasing the frequency of the injected pulse enhances the spatial resolution of the method. Such an enhancement is more noticeable for the 0.4-mS/m soil compared to the 4-m/S soil, since the decrease in the wavelength between 1 MHz and 10 MHz for the former is more significant than for the latter. Additionally, the lower resolution obtained for the 1 MHz pulse and 0.4-mS/m soil presumably stems from the longer associated wavelength (approximately twice as large compared to that for the 4-mS/m soil and same frequency). In general, the shorter the wavelength of the applied signal in relation to the length of the electrode, the more accurate the method solution.

Finally, comparing the results obtained for the 4-mS/m and 0.4-mS/m soils, the curves associated with the first are generally broader due to the greater dispersion associated with the frequency-dependent losses. At any rate, the most notable finding from the results in Figure 6 is that for both soil conductivities the fault point was correctly located even using a 1-MHz pulse, suggesting that signals with a relatively low-frequency content could be used for fault location in grounding electrodes.

5.3. Influence of Defect Location

Figure 7 shows the obtained results for a hard fault, considering the defect at $x = 10$ m and $x = 25$ m along the electrode. A 10 MHz pulse is injected and two soil conductivities are assumed, 4 mS/m and 0.4 mS/m.
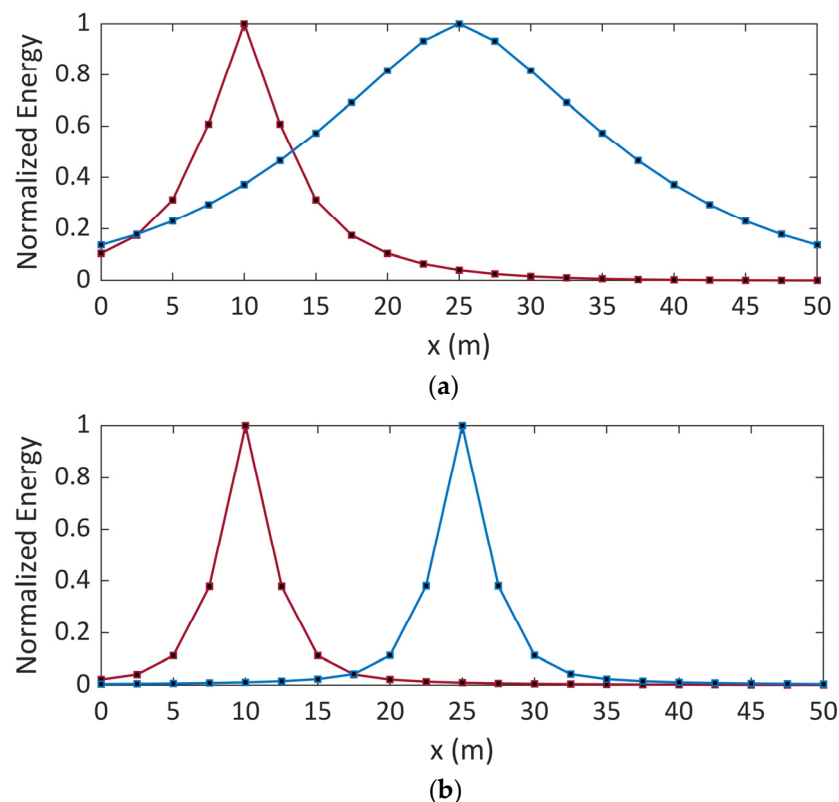
(**a**)

(**b**)

Figure 7. Normalized energy as a function of the position along the electrode considering distinct locations of the hard fault and soil conductivities of (**a**) 4 mS/m and (**b**) 0.4 mS/m. Red curve (defect at $x = 10$ m), blue curve (defect at $x = 25$ m).

According to the results, assuming a hard fault, it was possible to successfully locate the fault in both considered defect points and for both soil conductivities. For the 4-mS/m soil, moving from $x = 10$ m to $x = 25$ m, a significant increase in the curve width is observed. This effect, not seen for the 0.4 mS/m case, stems from the fact that, for points farther from the signal injection point, the effects of the frequency-dependent losses become more pronounced. This suggests that locating faults far from the signal injection point on very long electrodes buried in high-conductivity soils may be critical. On the other hand, long

electrodes are not expected in high-conductivity soils, since shorter electrodes are generally sufficient to achieve a satisfactory grounding resistance value (typically below 10 Ω).

5.4. Locating Soft Faults

Figure 8 shows the results obtained now considering a soft fault at x = 10 m and x = 25 m. A 10 MHz pulse is injected and two soil conductivities are assumed, 4 mS/m and 0.4 mS/m. As previously mentioned, a soft fault in a grounding electrode may be related to a corrosion process that causes the wire to deteriorate, leading to a decrease in its cross-section. As the impedance discontinuity introduced in this case is less strong than in the case of a breakpoint, this defect can be classified as a soft fault.
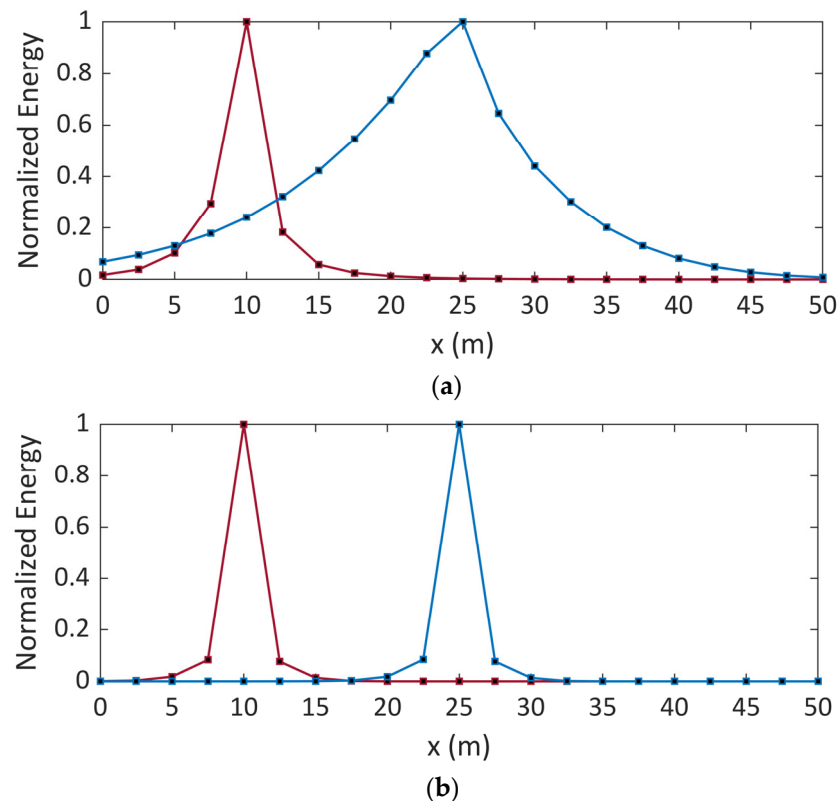

(a)

(b)

Figure 8. Normalized energy as a function of the position along the electrode considering distinct locations of the soft fault and soil conductivities of (**a**) 4 mS/m and (**b**) 0.4 mS/m. Red curve (defect at $x = 10$ m), blue curve (defect at $x = 25$ m).

As can be observed from the results, the proposed method was able to locate the soft fault at both assumed fault points and for the two ground conductivities considered, even though this fault introduced a nondiscernible modification in the grounding input impedance, as shown in Figure 3. This remarkable performance of the proposed method presumably stems from the strong focusing property of the EMTR-based locating algorithms. Finally, it is worth mentioning that the so-called reflectometry-based techniques for wire defect detection and location are not able to efficiently deal with the problem of soft defect detection and with wires immersed in lossy media, as reported in the literature [37]. These aspects are overcome with the use of the EMTR-based algorithm, mainly considering its focusing property and the possibility to deal with losses by applying the appropriate back-propagation model.

6. Discussion and Conclusions

In this paper, we carried out a theoretical analysis of the feasibility of applying the electromagnetic time reversal technique to locate faults in grounding systems. In the analyses, a horizontal grounding electrode buried in low- and high-conductivity soils was

assumed, and the locations of soft and hard faults at different points along the electrode were evaluated. The results obtained illustrated the basic principle and the possibilities offered through the use of the EMTR method for detecting and locating soft defects and breakpoints in grounding electrodes.

In the carried-out simulations, Gaussian pulses of frequencies between 1 MHz and 10 MHz were applied. Even for a 1 MHz pulse, satisfactory fault detection and location results were obtained, suggesting that the technique can be applied in practice without the need of deploying expensive and fast electronic devices and strict EMC constraints. It is worth noting that the higher the frequency of the applied pulse, the narrower the peaks indicating the fault point. Thus, for a high spatial resolution, larger bandwidths may be necessary. However, this does not seem to be an issue since, in most applications in grounding systems, what is most important is knowing that there is a defect and its approximate location.

An important result of the analyses presented in this paper is that the EMTR method proved to be efficient for locating faults in grounding electrodes, even though they are immersed in a medium with non-negligible losses. In fact, for the study at hand, the losses raise two main issues. The first corresponded to the fact that both Maxwell's equations and the telegrapher's equations are not rigorously time reversal invariant if we consider dissipative media. To deal with this, three different back-propagation models were tested, and it was shown that the inverted-loss BP model was able to correctly locate the fault point for both low- and high-conductivity soils. The second issue corresponds to the need to detect the signal reflected by the fault point, which, depending on the losses, can be difficult to measure. Figure 9 shows the reflected signal generated by a breakpoint in the middle of the same horizontal electrode analyzed in the paper buried in a soil of conductivity of 0.4 mS/m, and assuming the application of a 1-V, 10-MHz Gaussian pulse. It is seen that the amplitude of the reflected signal is of the order of a few hundreds of mV, which is easily detectable using appropriate signal conditioners. In the case of a soft fault, a reflected signal of lower amplitude is expected, although still detectable. In this case, the amplitude of the signal depends on the degree of the impedance discontinuity, which, in case of a lossy medium, is frequency dependent. Finally, in the case of longer electrodes buried in high-conductivity soils, where losses play an important role, a multiport characterization of the grounding electrode might improve the efficiency of the technique. Furthermore, the portable impulse generators developed in [38], which produce output voltages of up to approximately 1 kV, could be used to improve the signal-to-noise ratio.
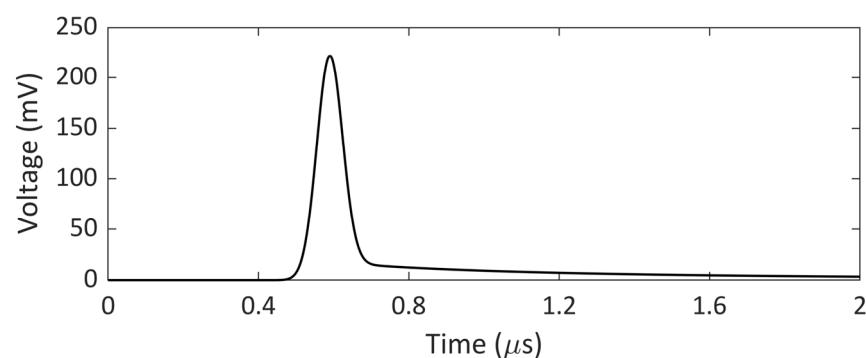

Figure 9. Reflected signal from a breakpoint in the middle of a 50 m long electrode buried in soil of 0.4 mS/m.

The proposed technique was applied to a simple horizontal electrode arrangement, which is representative of tower-foot grounding systems of power lines and buried wires used for the interconnection of grounding systems for wind turbines on wind farms. However, it can immediately be extended to other arrangements, such as ring earth electrodes, typically used in lightning protection systems (LPSs) of buildings, and arrangements that have a few crossing points, such as four-star electrode arrangements. In the case of more

complex arrangements, for example, substation grounding grids, due to the presence of multiple junctions, which introduce additional intrinsic impedance discontinuities, a more complex signal processing method should be implemented. Alternatively, a more powerful EMTR technique could be applied, such as the time reversal multiple-signal classification (TR-MUSIC). In [27], considering a scenario where losses were negligible, the TR-MUSIC was shown to be a promising technique to locate faults in complex cable networks.

Compared to other methods for diagnosing defects in grounding systems, the proposed method can be straightforwardly applied considering its single experimental step that corresponds to applying a probe impulse voltage to one terminal of the potentially faulty electrode and recording the resultant transient signal at the same terminal from which the reflected signal from the defect point can be extracted. Since the measurement can be carried out on a single-electrode terminal or on a few terminals if it is necessary to increase the accuracy of the method, there is no need to move the measurement setup along the entire route of the buried electrodes, such as what is required in electromagnetic methods, which may be unfeasible, for example, in overhead lines depending on the site where the structures are located. A further advantage of the proposed EMTR-based method is that it proved to be able to also localize soft faults, which may be related to initial or intermediate corrosion processes, allowing to anticipate maintenance in grounding systems. Locating such soft faults is very difficult using traditional techniques, such as the network method, or through simply measuring the grounding resistance. In the case of electromagnetic methods, the analysis of the output data for the classification of the type of fault (hard or soft) is often performed manually, and it can be affected by the experience of the engineer or, if performed using computational tools, it might depend on the algorithm used for the classification.

Based on the above considerations and discussions, the proposed method appears to be very promising for real applications. In Appendix A, a first proposal on how the proposed method could be applied in practice to locate defects in grounding electrodes is presented. Finally, the authors are involved in experimental developments to confirm the application of the proposed technique for locating faults in grounding electrodes.

Author Contributions: Conceptualization, R.A., N.D., H.K., M.R. and F.R.; methodology, R.A., N.D., H.K., M.R. and F.R.; software, R.A.; validation, R.A. and N.D.; formal analysis, R.A. and N.D.; investigation, R.A. and N.D.; resources, F.R.; data curation, R.A.; writing—original draft preparation, R.A. and N.D.; writing—review and editing, H.K., M.R. and F.R.; visualization, R.A.; supervision, M.R. and F.R.; project administration, M.R. and F.R.; funding acquisition, R.A., N.D. and F.R. All authors have read and agreed to the published version of the manuscript.

Data Availability Statement: Not applicable.

Appendix A. Practical Application of the Proposed Method to Locate Defects in Grounding Electrodes

This Appendix A presents a first proposal on how the proposed method could be applied in practice to locate defects in grounding electrodes. In the following, it is assumed that the basic geometrical characteristics of the grounding electrode, namely, the electrode radius and length, are known from design information. It is also assumed that the soil characteristics can be obtained from local measurements. The following steps summarize the application of the method in practice. The mathematical operations were defined in the time domain, although they can also be performed in the frequency domain.

1.   An impulse voltage is applied between the potentially faulty electrode and an auxiliary electrode (current return electrode), as shown in Figure A1. The frequency content of the applied signal must be defined according to the desired spatial resolution

for the fault location. The resultant voltage at the left end of the faulty electrode, $v_{ed}(t)$, is recorded using a measurement system. Such a system could be as simple as an oscilloscope or a sophisticated data acquisition system. The distance between the electrode under test and the current return electrode should be sufficient to avoid mutual coupling between them. Additionally, to minimize the electromagnetic coupling between the voltage and current leads, they are orthogonally positioned.

2.   By means of a numerical simulation, the same impulse voltage is applied between the grounding electrode without a defect and the current return electrode, and the voltage at its left end $v_e(t)$ is computed. From the measured voltage $v_{ed}(t)$ and the simulated voltage $v_e(t)$, the reflected signal from the fault point, $v_{rd}(t)$, can be determined. Additionally, from numerical simulations, the spatial voltage distribution along the electrode without a defect, $v_e(t, x)$, is determined.

3.   The reflected signal $v_{rd}(t)$ is time-reversed and back-injected through a numerical simulation into the grounding electrode without a defect and the spatial voltage distribution, $v_{ed}(t, x)$, is determined.

4.   The signals $v_e(t, x)$ and $v_{ed}(t, x)$ are convoluted at each point x along the electrode. This product is expected to reach a maximum at the defect point.
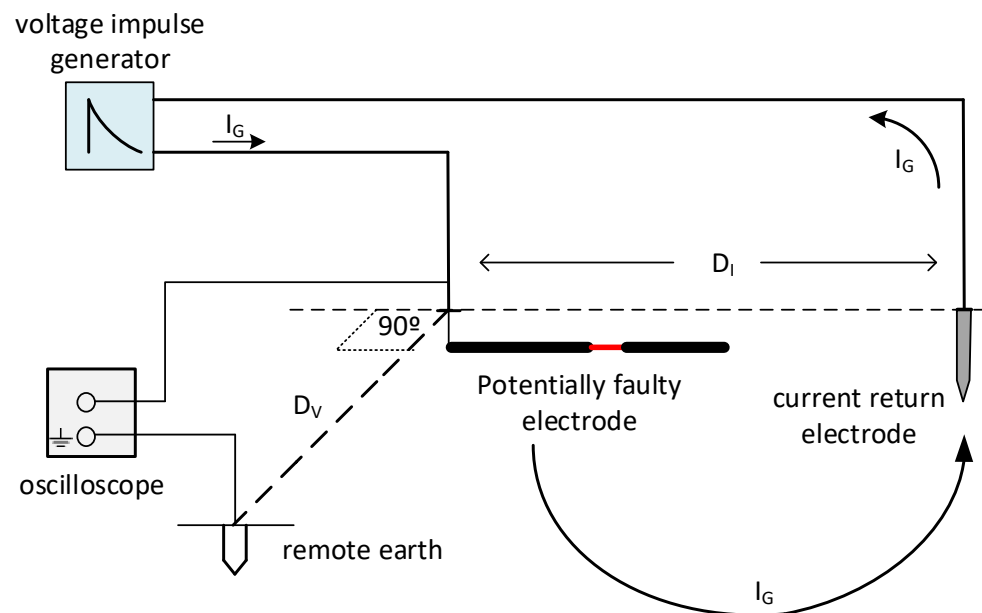

Figure A1. Experimental setup to locate defects in grounding electrodes.

References

1.   *IEEE Std 80*; Guide for Safety in AC Substation Grounding. Institute of Electrical and Electronics Engineers (IEEE): New York, NY, USA, 2015.
2.   *IEC 62305*; Protection against Lightning. International Electrotechnical Commission (IEC): Geneva, Switzerland, 2010.
3.   Durham, R.A.; Szczecinski, S.J.; Durham, M.O. Factors Impacting Selection of Grounding and Bonding Conductors. *IEEE Trans. Ind. Appl.* **2020**, *56*, 4652–4661. [CrossRef]
4.   He, J.; Zeng, R.; Zhang, B. *Methodology and Technology for Power System Grounding*, 1st ed.; John Wiley & Sons, Ltd.: Singapore, 2013; ISBN 9781118254950.
5.   Zhang, Z.; Ye, H.; Dan, Y.; Duanmu, Z.; Deng, J.; Gao, C.; Gan, P. Study on Corrosion Fracture Diagnosis Method of Grounding Wire of Tower Grounding Device. *Measurement* **2020**, *166*, 108213. [CrossRef]
6.   Lu, C.; Zhang, T.; Sun, S.; Cao, Z.; Xin, M.; Fu, G.; Wang, T.; Wang, X. Fault Diagnosis of Tower Grounding Conductor Based on the Electromagnetic Measurement and Neural Network. *IEEE Trans. Instrum. Meas.* **2022**, *71*, 1–9. [CrossRef]
7.   Zhang, C.; Liao, Y.; Gao, X.; Zhao, J.; Yuan, Y.; Liao, R. Research Advances of Soil Corrosion of Grounding Grids. *Micromachines* **2021**, *12*, 513. [CrossRef] [PubMed]
8.   Dawalibi, F. Electromagnetic Fields Generated by Overhead and Buried Short Conductors Part 2—Ground Networks. *IEEE Trans. Power Deliv.* **1986**, *1*, 112–119. [CrossRef]

9. Yu, C.; Fu, Z.; Hou, X.; Tai, H.-M.; Su, X. Break-Point Diagnosis of Grounding Grids Using Transient Electromagnetic Apparent Resistivity Imaging. *IEEE Trans. Power Deliv.* **2015**, *30*, 2485–2491. [CrossRef]

10. Yu, C.; Fu, Z.; Wang, Q.; Tai, H.-M.; Qin, S. A Novel Method for Fault Diagnosis of Grounding Grids. *IEEE Trans. Ind. Appl.* **2015**, *51*, 5182–5188. [CrossRef]

11. Song, H.; Dong, H.; Wang, X.; Tang, L. Non-Destructive Diagnosis of Grounding Grids Based on the Electromagnetic Induction Impedance Method. *Meas. Sci. Technol.* **2021**, *32*, 115901. [CrossRef]

12. Zhang, X.-L.; Zhao, X.-H.; Wang, Y.-G.; Mo, N. Development of an Electrochemical in Situ Detection Sensor for Grounding Grid Corrosion. *Corrosion* **2010**, *66*, 076001–076007. [CrossRef]

13. Hu, J.; Zeng, R.; He, J.; Sun, W.; Yao, J.; Su, Q. Novel Method of Corrosion Diagnosis for Grounding Grid. In Proceedings of the PowerCon 2000 International Conference on Power System Technology (Cat. No. 00EX409), Perth, Australia, 4–7 December 2000; Volume 3, pp. 1365–1370.

14. Zheng, R.; He, J.; Hu, J.; Lu, G.; Luo, B. The Theory and Implementation of Corrosion Diagnosis for Grounding System. In Proceedings of the Conference Record of the 2002 IEEE Industry Applications Conference, 37th IAS Annual Meeting (Cat. No. 02CH37344), Pittsburgh, PA, USA, 13–18 October 2002; Volume 2, pp. 1120–1126.

15. Fink, M. Time Reversal of Ultrasonic Fields. I. Basic Principles. *IEEE Trans. Ultrason. Ferroelectr. Freq. Control* **1992**, *39*, 555–566. [CrossRef]

16. Wu, F.; Thomas, J.-L.; Fink, M. Time Reversal of Ultrasonic Fields. Il. Experimental Results. *IEEE Trans. Ultrason. Ferroelectr. Freq. Control* **1992**, *39*, 567–578. [CrossRef] [PubMed]

17. Cassereau, D.; Fink, M. Time-Reversal of Ultrasonic Fields. III. Theory of the Closed Time-Reversal Cavity. *IEEE Trans. Ultrason. Ferroelectr. Freq. Control* **1992**, *39*, 579–592. [CrossRef] [PubMed]

18. Rachidi, F.; Rubinstein, M.; Paolone, M. (Eds.) *Electromagnetic Time Reversal: Application to Electromagnetic Compatibility and Power Systems*, 1st ed.; John Wiley & Sons, Ltd.: Hoboken, NJ, USA, 2017.

19. Lugrin, G.; Parra, N.M.; Rachidi, F.; Rubinstein, M.; Diendorfer, G. On the Location of Lightning Discharges Using Time Reversal of Electromagnetic Fields. *IEEE Trans. Electromagn. Compat.* **2014**, *56*, 149–158. [CrossRef]

20. Razzaghi, R.; Lugrin, G.; Manesh, H.M.; Romero, C.; Paolone, M.; Rachidi, F. An Efficient Method Based on the Electromagnetic Time Reversal to Locate Faults in Power Networks. *IEEE Trans. Power Deliv.* **2013**, *28*, 1663–1673. [CrossRef]

21. Razzaghi, R.; Lugrin, G.; Rachidi, F.; Paolone, M. Assessment of the Influence of Losses on the Performance of the Electromagnetic Time Reversal Fault Location Method. *IEEE Trans. Power Deliv.* **2017**, *32*, 2303–2312. [CrossRef]

22. Codino, A.; Wang, Z.; Razzaghi, R.; Paolone, M.; Rachidi, F. An Alternative Method for Locating Faults in Transmission Line Networks Based on Time Reversal. *IEEE Trans. Electromagn. Compat.* **2017**, *59*, 1601–1612. [CrossRef]

23. Wang, Z.; He, S.; Li, Q.; Liu, B.; Razzaghi, R.; Paolone, M.; Xie, Y.; Rubinstein, M.; Rachidi, F. A Full-Scale Experimental Validation of Electromagnetic Time Reversal Applied to Locate Disturbances in Overhead Power Distribution Lines. *IEEE Trans. Electromagn. Compat.* **2018**, *60*, 1562–1570. [CrossRef]

24. Razzaghi, R.; Scatena, M.; Sheshyekani, K.; Paolone, M.; Rachidi, F.; Antonini, G. Locating Lightning Strikes and Flashovers along Overhead Power Transmission Lines Using Electromagnetic Time Reversal. *Electr. Power Syst. Res.* **2018**, *160*, 282–291. [CrossRef]

25. El Sahmarany, L.; Berry, L.; Kerroum, K.; Auzanneau, F.; Bonnet, P. Time-Reversal for Wiring Diagnosis. *Electron. Lett.* **2012**, *48*, 1343. [CrossRef]

26. Kafal, M.; Cozza, A.; Pichon, L. Locating Multiple Soft Faults in Wire Networks Using an Alternative DORT Implementation. *IEEE Trans. Instrum. Meas.* **2016**, *65*, 399–406. [CrossRef]

27. Kafal, M.; Cozza, A.; Pichon, L. Locating Faults With High Resolution Using Single-Frequency TR-MUSIC Processing. *IEEE Trans. Instrum. Meas.* **2016**, *65*, 2342–2348. [CrossRef]

28. Karami, H.; Azadifar, M.; Mostajabi, A.; Rubinstein, M.; Karami, H.; Gharehpetian, G.B.; Rachidi, F. Partial Discharge Localization Using Time Reversal: Application to Power Transformers. *Sensors* **2020**, *20*, 1419. [CrossRef]

29. Ragusa, A.; Sasse, H.G.; Duffy, A.; Rubinstein, M. Application to Real Power Networks of a Method to Locate Partial Discharges Based On Electromagnetic Time Reversal. *IEEE Trans. Power Deliv.* **2022**, *37*, 2738–2746. [CrossRef]

30. Sunde, E.D. *Earth Conduction Effects in Transmission Systems*; Dover Publications: New York, NY, USA, 1968.

31. King, R. Antennas in Material Media near Boundaries with Application to Communication and Geophysical Exploration, Part I: The Bare Metal Dipole. *IEEE Trans. Antennas Propag.* **1986**, *34*, 483–489. [CrossRef]

32. Schelkunoff, S.A. The Electromagnetic Theory of Coaxial Transmission Lines and Cylindrical Shields. *Bell Syst. Tech. J.* **1934**, *13*, 532–579. [CrossRef]

33. Grcev, L.; Grceva, S. On HF Circuit Models of Horizontal Grounding Electrodes. *IEEE Trans. Electromagn. Compat.* **2009**, *51*, 873–875. [CrossRef]

34. Paul, C.R. *Analysis of Multiconductor Transmission Lines*, 2nd ed.; John Wiley & Sons, Inc.: Hoboken, NJ, USA, 2008.

35. Tesche, F.M.; Ianoz, M.V.; Karlsson, T. *EMC Analysis Methods and Computational Models*; Wiley: New York, NY, USA, 1997.

36. Grcev, L. Impulse Efficiency of Ground Electrodes. *IEEE Trans. Power Deliv.* **2009**, *24*, 441–451. [CrossRef]

37. Auzanneau, F. Wire Troubleshooting and Diagnosis: Review and Perspectives. *Prog. Electromagn. Res. B* **2013**, *49*, 253–279. [CrossRef]
38. Alipio, R.; Coelho, V.L.; Canever, G.L. Experimental Analysis of Horizontal Grounding Wires Buried in High-Resistivity Soils Subjected to Impulse Currents. *Electr. Power Syst. Res.* **2023**, *214*, 108761. [CrossRef]